A comparison of pad metallization in miniaturized microfabricated silicon microcantilever-based wafer probes for low contact force low skate on-wafer measurements

Khadim Daffe, Jaouad Marzouk, Christophe Boyaval, Gilles Dambrine, Kamel Haddadi, S. Arscott

PAPER

A comparison of pad metallization in miniaturized microfabricated silicon microcantilever-based wafer probes for low contact force low skate on-wafer measurements

IOP Publishing Journal of Micromechanics and Microengineering
J. Micromech. Microeng. **32** (2022) 015007 (13pp) https://doi.org/10.1088/1361-6439/ac3cd7

A comparison of pad metallization in miniaturized microfabricated silicon microcantilever-based wafer probes for low contact force low skate on-wafer measurements

Khadim Daffe, Jaouad Marzouk, Christophe Boyaval, Gilles Dambrine, Kamel Hadaddi and Steve Arscott*

University of Lille, CNRS, Centrale Lille, University Polytechnique Hauts-de-France, UMR 8520-IEMN, F-59000 Lille, France

E-mail: steve.arscott@univ-lille.fr

Received 27 July 2021, revised 22 October 2021
Accepted for publication 24 November 2021
Published 8 December 2021

Abstract

Miniaturized, microfabricated microelectromechanical systems-based wafer probes are used here to evaluate different contact pad metallization at low tip forces (<mN) and low skate on the on-wafer pads. The target application is low force RF probes for on-wafer measurements which cause minimal damage to both probes and pads. Low force enables the use of softer, more conductive metallisation. We have studied four different thin film contact pad metals based on their thin film electrical resistivity and micro-hardness: gold, nickel, molybdenum, and chromium. The contact pads sizes were micrometre ($1.9 \times 1.9\ \mu m^2$) and sub-micrometre ($0.6 \times 0.6\ \mu m^2$). The contact resistance of Au–Au, Ni–Au, Mo–Au, and Cr–Au was measured as a function of tip deflection. The tip force (loading) of the contacts was evaluated from the deflection of the cantilever. It was observed that an overtravel of 300 nm resulting in a contact force of $\sim$400 μN was sufficient to achieve a contact resistance <1 Ω for a sub-micrometre gold contact pad. Our results are compared with an analytical model of contact resistance in loaded metal-metal contacts—a reasonable fit was found. A larger contact resistance was observed for the other metals—but their hardness may be advantageous when probing other materials. Using a combination of a rigid silicon cantilever (>1000 Nm^{-1}) and small contact pads enabled us to show that it is the length of the pad (in contact with the surface) which determines the contact resistivity rather than the total contact pad area.

Keywords: microelectromechanical systems, silicon microsystems, microcantilever, on-wafer probe, contact resistance, microwave probe, microfabrication

(Some figures may appear in colour only in the online journal)

* Author to whom any correspondence should be addressed.

1. Introduction

Wafer probing from DC to millimetre-wave measurements is routinely performed using commercially-available, prefabricated parts-assembled ground-signal-ground (GSG) probes [1]. The minimum pad size for manual probe placement is 25 $\times$ 35 μm. The recommended minimum pad size for general use (auto or semi-auto probe placement) is 50 μ $\times$ 50 μm. For narrow pitch probes (e.g. 50 or 75 μm pitch) minimum pad size is 30 μ $\times$ 50 μm. Due to an evident size discrepancy, such probes cannot be directly placed onto devices which are situated on a planar substrate. On-wafer measurements require special areas on chips which include large test pads and lines connected to smaller devices—these areas consume valuable chip area. In addition, such large pads and lines introduce parasitic elements whose behaviour can dominate the devices-under-test. At higher measurement frequencies both parasitic elements and chip area wastage could be avoided by being able to accurately and precisely place correctly-calibrated, suitably-miniature probes directly onto devices [2]. Unfortunately, the prefabricated parts/assembly-based manufacturing process used for the assembling of macroscopic wafer probes does not lend itself well to miniaturization. In contrast, a microtechnology fabrication (microfabrication) approach has been shown to provide a manufacturing solution for the miniaturization of such probes; where the precise control of probe dimensions and their layout is essential for optimized performance.

There is a currently need for a new generation of miniaturized probes for the on-wafer characterization of microwave integrated circuits over a wide range of frequencies [3–6]. Such probes require small pitches, reduced contact pad surfaces, controlled contact forces, high touchdown precision, high repeatability, and higher measurement accuracy and resolution than their current macroscopic commercial counterparts. Measurements using direct on-wafer probing provide rapid feedback on the overall status of a fabrication process and enables the implementation of accurate modelling. Commercial macroscopic GSG probes are commonly used for on-wafer characterization of microwave frequency band (1–1000 GHz) devices [1, 7]. However, in many cases, conventional RF probes cannot now meet industry's evolving standards. The 'cost per touchdown' of current probes is relatively high. Also, current macroscopic probes have a contact pad surface of the order of hundreds of square micrometres associated with a pitch (spacing between probe contact pads) dimension between tens and hundreds of micrometres. These critical dimensions, added to prober positioning accuracies, requires on-wafer devices with pad sizes to be of the order of at least several tens of micrometres for on-wafer characterization. In general, such dimensions imply sizeable capacitance, and inductance parasitic effects in the RF characterization of nanoscale electronic components. These parasitic effects can cause measurement inaccuracies by screening the intrinsic properties of nanometre-sized devices. It is thus necessary to improve RF probe technology via a scaling down of dimensions to be able to characterize future generations of electronic devices that will include miniaturized pads and lines. Probes can be broken down into two types: (a) macroscopic, manually-assembles probes and (b) micro (even nano) fabricated probes. In terms of ultimate size and scaling, the former approach has been very successful up until now but has limitations in the sub-10 μm regime. The latter approach does not suffer from size and scaling issues—current lithographic methods can reach <10 nm—but creates other issues: probe fragility, positioning and touchdown precision, contact force optimisation, electrical contact quality, and wear and repeatability issues. Despite these challenges, applying micro and nanotechnology has proven to be of great use in other probing areas, e.g. all near-field microscopies.

As early as 1988 Leslie and Matta [8] developed a metallized dielectric membrane card technology capable of robust testing of aluminium pads up to 2.5 GHz. Following this, in 1989 Hong *et al* [9, 10], working at Stanford, were the first to report use of a metallized silicon membranes (~5–20 μm thick) obtained using microtechnology—the probes were tested up to 20 GHz. Edward Godshalk [11] (working at Cascade Oregon USA) lithographically fabricated a W-band (75–110 GHz) GSG probe based on metallization (10 μm thick gold lines) of an alumina substrate. In 1995, using bulk micromachining, Beiley *et al* [12, 13] developed a membrane-based probe card. Contact probes were as small as 10 μm square—the probes were tested up to 20 GHz. Somewhat ahead of their time, Safwat *et al* [14] fabricated a GSG probe based on a lithographically-patterned metallized polyamide flexible membrane. The specific probe metallization was not given, but they underlined the problems of small probes, lower forces, and—importantly—oxidized aluminium pads. Following this, Chun *et al* [15] used a microelectromechanical systems (MEMS) approach to produce a robust 'interposer' probing device functioning up to 10 GHz. Itoh *et al* [16] using microtechnology to produce specifically-designed bent and buckled metal (Ni) microcantilevers. Itoh *et al* [17] and Kim *et al* [18] furthered bent/buckled microcantilever-based probes for on-chip testing. In 2006 Tsou *et al* [19] used bulk silicon micromachining to fabricated IC test probes based on controlled buckled microcantilevers—DC testing. 2008 Liu *et al* [20] also used silicon micromachine to produce a sophisticated array of probes—the contact area was 1 μm^2—again, DC testing. In 2009, Wang *et al* [21] used a combination of silicon bulk micromachining to demonstrate out-of-plane nickel-based probes for on-wafer testing.

However, it was not until 2010 that Reck *et al* [22] concisely described the problem of applying silicon micromachining for the development of miniaturized GSG probes for on-chip microwave measurements. They expounded the importance of a combined electromagnet/mechanical approach together with the contact force at the touchdown pads. Following this, in 2011 Reck *et al* [23, 24] described many of these ideas in detail—pointing the way for many years of research, they produced prototype micromachined GSG probes tested up to 750 GHz—effectively challenging, and then working with, commercial probe suppliers. Chen *et al* [25] studied the repeatability and reliability of silicon micromachined GSG probes. They showed that 2 $\times$ 10^5 contact cycles demonstrated a <0.6 dB measurement variation up to 750 GHz.

Their touchdown contact pad size was ∼20 μm. Going further, Yu *et al* [26, 27] demonstrated a prototype integrated strain sensor in silicon micromachined GSG microwave probes. The goal was to control contact force for optimised electrical contact and probe measurement repeatability. Yuan *et al* [28] proposed an interesting approach for micromachined probes using flexible materials. Using PDMS with metallized through holes they were able to demonstrate on-wafer probing up to 10 GHz. In 2014 Bauwens *et al* [29, 30] reported first characterization (>1 THz) of microfabricated silicon-based GSG probes. In 2014 Marzouk *et al* [31] presented a design guide (combined mechanical and electromechanical modelling) for miniaturized GSG probes based on thin silicon cantilevers—considering the impact of mechanical deflection of the silicon microcantilever on the probe microwave performance and touchdown contact force. Marzouk *et al* [32] demonstrated micromachined probes and their stand-alone characterization. In 2015 Marzouk *et al* [33] presented the full microfabrication process for miniaturized GSG silicon microcantilever-based probes—2 μm^2 contacts pitch 4.5 μm. Using these microprobes Fellali *et al* [2] using such probes demonstrated a gain in terms of parasitic elements. Haddadi *et al* [34, 35] using the probes produced a robotic positioning inside a scanning electron microscope (SEM) and their on-wafer characterization up to 40 GHz [36]. Marzouk *et al* [37] used such probes to demonstrate 6000 touchdowns and a contact resistance of <1 Ω despite the very low contact pad size. Marzouk *et al* [38] also showed contact resistance vs contact force for the optimization of measurements. In 2017 Marzouk *et al* [39] used the probe to measure a III–V nanowire. In 2020, Marzouk *et al* [40] demonstrated the importance of surface-associated losses in miniaturized silicon-based GSG probes. In 2020 Taleb *et al* [41] detailed the critical factors involved in the positioning of small probes onto circuits—illustrating the importance of contact quality. Zhang *et al* [42] demonstrated a w-band micromachined on-wafer probe with an integrated balun. In 2017 Barker *et al* [43] noted the advantages of high-resistivity silicon-on-insulator (SOI) as a platform for THz circuits including miniature probes. Using silicon microtechnology, Gonzalez *et al* [44] demonstrated a simple replaceable tip technology (0–40 GHz). Zhang *et al* [45] described the first-reported development of a micromachined differential probe for direct on-wafer measurements operating in the 140–220 GHz frequency band. In 2019 Zhang *et al* [46] demonstrated the first differential on-wafer probe with integrated balun operating in the 220–330 GHz band. It has very recently been pointed out that GSG probes can have a number of side effects during measurements [47, 48].

Wear of the contact surfaces occurs during repeated physical contacting of the two metals. Wear results in the continual loss of material from surfaces; this results in changes of the probes dimensions and damage to on-wafer pads. If the required contact force is high, the technological solution is to employ more robust contact metallisation, e.g. alloys. By reducing the contact force required to obtain a suitable contact resistance, softer more conductive mentalisations can be envisaged.

In the development of RF probes for on-wafer measurements, one area that needs addressing is the electrical performance of small metal contact pads (micrometre and sub-micrometre) integrated into microfabricated probes and their behaviour as the probe is put into contact with chip pads by using a contact force generated by a microcantilever deflection to achieve an optimal, minimal skate/minimal damage metal-to-metal contact. The present article addresses some of these issues. The central idea here is to characterize the contact resistance of micrometre and sub-micrometre-sized contact pads at DC of cantilever-based MEMS probes which are destined for RF on-wafer measurements.

2. Microfabrication of the probes having sub-micrometre contact pads

2.1. Microfabrication process

Miniaturized GSG wafer probes were fabricated for the study using a multi-step microfabrication process developed by the authors [33]. The process is based on the principles of surface [49] and bulk [50] micromachining of silicon which enables the fabrication of MEMS [51] structures such as microcantilevers [52]. The principal difference here with our previous work is the final metallization step of the process. This final metallization step defines the three small, square contact pads at the end of the GSG probe tip. By dividing the 3 inch diameter high-resistivity (>1000 Ω cm) SOI wafer (Si-Mat, Germany) into four parts, we were able to perform a lithographic/lift-off/evaporation metallization of four different contact pad metals (gold, molybdenum, nickel, and chromium) onto the probe structures. The wafer design included 192 probes for high-frequency measurements, 160 probes for DC characterization, 100 back-to-back probes, and various coplanar transmission lines. Despite being a relatively small-diameter SOI wafer, this still demonstrates the power of this batch-manufacturing approach for such probes. The design of the coplanar waveguides (CPW) on the probes was achieved using numerical modelling taking into account the mechanical deformation of the microcantilever when the probe is in use [31]. The reason for the choice of these four metals will be described in the following section. Figure 1(a) shows a SEM image of a typical probe fabricated for the study (the contact pads are nickel in this case). The microfabricated GSG wafer probes are composed of a gold (500 nm thick) CPW running partly on a thick silicon (thickness = 400 μm) support chip and partly on a triangular-shaped silicon microcantilever (length = 400 μm, thickness = 20 μm). The lines on the microcantilever run up to the probe tip where the three square GSG contact pads are situated. Once the silicon microcantilevers are back-etched, the probes are removed from the silicon wafer and stored in a gel box—see figures 1(b) and (c). In addition to investigating the type of contact metal, lithography enabled us to investigate the contact size. The contact pads of the probes had two dimensions: 0.6 × 0.6 μm^2 and 1.9 × 1.9 μm^2. The optimized, stable microfabrication process ensured that the probe device yield was near to

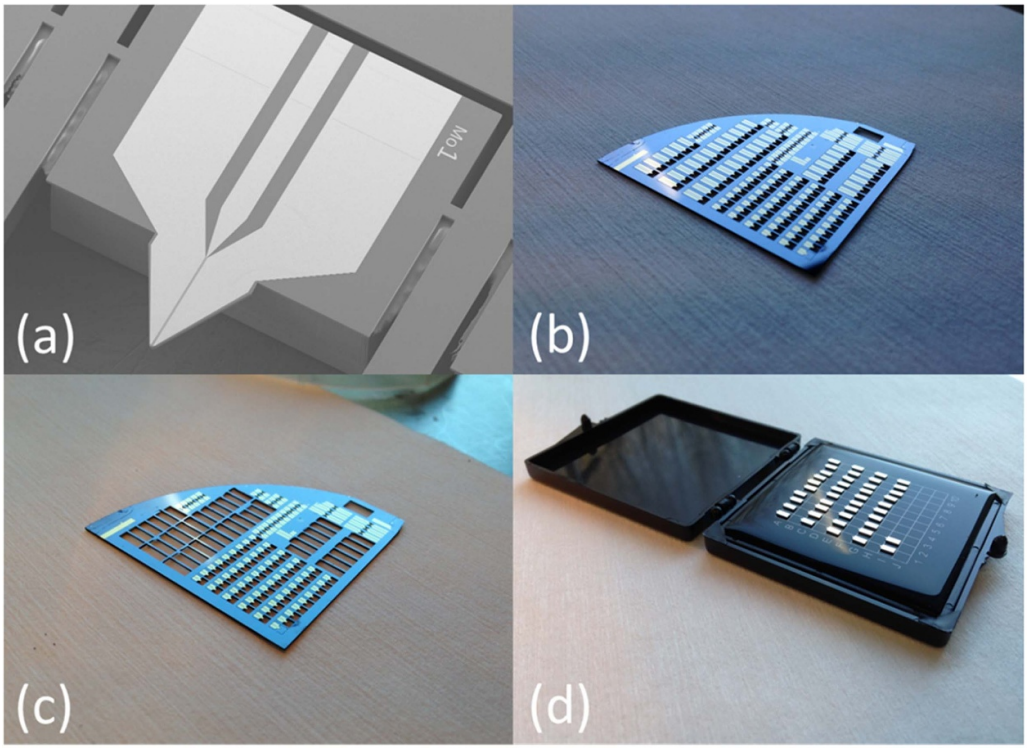

Figure 1. Results of the microfabrication of the miniature wafer probes. (a) SEM image of a an example of a miniaturized GSG wafer probe fabricated using our microfabrication process [33] using commercial high-resistivity SOI wafers. Gold CPW runs on a silicon support chip and over a triangular microcantilever. The CPW leads up to small GSG contact pads having dimension of 0.6 × 0.6 μm and 1.9 × 1.9 μm. (b) Photograph of a quarter of the silicon wafer with back-etched released silicon microcantilevers and (c) the quarter of the silicon wafer with the probes removed and (d) put into a gel box. Reproduced from [33].

100%—demonstrating another advantage of batch fabrication. Despite this, one could occasionally observe a thin, brittle silicon membrane in the small gaps of the deep etch due to an uneven etch rate [53]. Fortunately, these did not create a problem when cleaving the probes—nor did they affect the employment of the probes for measurements.

2.2. Choice of the GSG contact pad metals

We chose four contact pad metals (gold, molybdenum, nickel, and chromium) having different values of electrical resistivity ρ, mechanical hardness H, and surface roughness Ra. These are three physical parameters known to govern the behaviour of a metal-to-metal electrical contact under an applied external force/load [54, 55]. A metal-to-metal electrical junction is physically composed of contacting asperities (conduction paths having a certain resistivity) which are determined by the surface roughness. Application of an external force/load to the metal-to-metal junction leads to mechanical deformation of the contacting asperities—this leads to an increase in the contact area. In choosing contact pad metals for probes one must also consider the predisposition of the metal to the formation of an oxide or nitride when the probe is not being used—these potentially-insulating layers can increase contact resistance. For example, silver has a low electrical resistivity, however when silver is exposed to air it develops a silver sulphide and oxide at the surface—these are likely to inhibit the quality of the contact with time. Some metals are not particularly 'planar-microtechnology friendly', e.g. the high-temperature evaporation of tungsten can cause technological problems during the lift-off patterning process. Iridium has been used in RF MEMS switches, but like silver, iridium forms an oxide on the surface when exposed to air—it is also not a particularly common lift-off thin film metal. We therefore chose four relatively common technological thin film metals. These metals enabled a study of the impact of resistivity, hardness, and roughness on performance of MEMS microwave probes—and were all relatively compatible with common microfabrication steps. Table 1 shows the properties relevant to the study of the metals used for the small contact pads.

Table 1. Electrical resistivity and hardness of the metals used to form the contact pads of the probes. The resistivities are bulk values—the hardness are values for thin films [56–59].

Contact pad metal	Resistivity ρ (nΩ m)	Hardness H (GPa)
Gold (Au)	22.1	1.5
Molybdenum (Mo)	53.4	11.3
Nickel (Ni)	69.3	8
Chromium (Cr)	125	9

Figure 2 shows the tips of the four types of probes fabricated for the study—indicating the probe contact pads and their respective metallization. In the four cases the contact pads are made of gold—figure 2(a), molybdenum—figure 2(b),

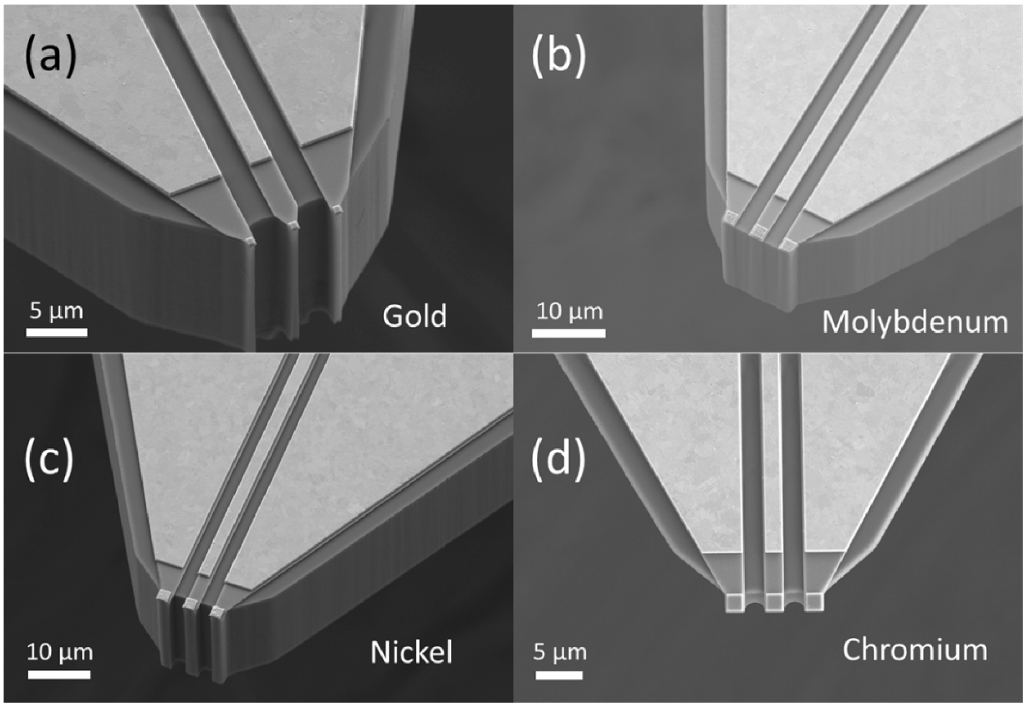

Figure 2. SEM images of the tips of the probes fabricated for the study. The small GSG contact metals are evaporated (a) gold, (b) molybdenum, (c) nickel, and (d) chromium. Contact pad dimensions $= 0.6 \times 0.6\ \mu m^2$ (Au), $1.9 \times 1.9\ \mu m^2$ (Mo, Ni, and Cr). The thickness of the metal pads was 0.5 μm.

nickel—figure 2(c), and chromium—figure 2(d). This figure highlights another design difference compared to a previous generation of microfabricated probes [33]. To ensure that only the three small square contact pads (or a portion of the pad area for low cantilever deflections) are in contact with the wafer-under-test, the three gold coplanar lines are halted at 5 μm from the contact pads—the interconnection between the lines and the contact pads is obtained via the underlying chromium layer. This element does not alter the measurement sensitivity/accuracy as the reference impedance of the measurement equipment, i.e. vector network analyser is 50 Ω, and micro- to nano-devices exhibit high impedance in the order of kilo-ohms. In other words, this element introduced a resistance of tens of ohms that is in favour of the electrical performance. The chip design also allowed the formation of probes where the contact pad areas were visible when viewing the rear side of the microcantilever to aide positioning of the probe—an example of this is given in figures 2(a) and (c).

As further evidence that the lift-off processes of the four different contact pad metals was successful, figure 3 shows images obtained in the SEM using back scattered electrons.

2.3. Surface roughness of the four GSG contact pad metals

Along with electrical resistivity and mechanical hardness, the surface roughness of a metal is known to play a key role in a metal-to-metal electrical contact [54, 55]. Atomic force microscopy (AFM) was used to measure the arithmetic average surface roughness (*Ra*) of the four small contact pad metals used in the study. During the evaporation of the contact pads, control samples composed of clean, flat silicon wafers were also deposited with the contact pad metal—the roughness of these coated surfaces were measured using AFM. A Dimension D3100 (Bruker–Veeco, USA) AFM was used for the measurements. Table 2 shows the evaporation rate used for the deposition of the thin films and values of *Ra* obtained from the AFM measurements on small surfaces comparable with the size of the contact pads on the probes.

3. Electrical characterization of the microfabricated probes

3.1. Probe mounting for electrical characterization

The silicon probes need to be fixed to a larger, robust PCB for the DC electrical measurements. We fabricated PCBs and used a combination of epoxy gluing and conductive paste to link the probe chip contacts to the PCB tracks. Figure 4 shows mounted probes ready for DC characterization. The CPW transitions have been considered to accommodate the DC measuring equipment to the CPW probe structure.

3.2. Electrical characterization of back-to-back microfabricated probes

Figure 5 shows an example of a back-to-back probing structure. The back-to-back probe configurations which

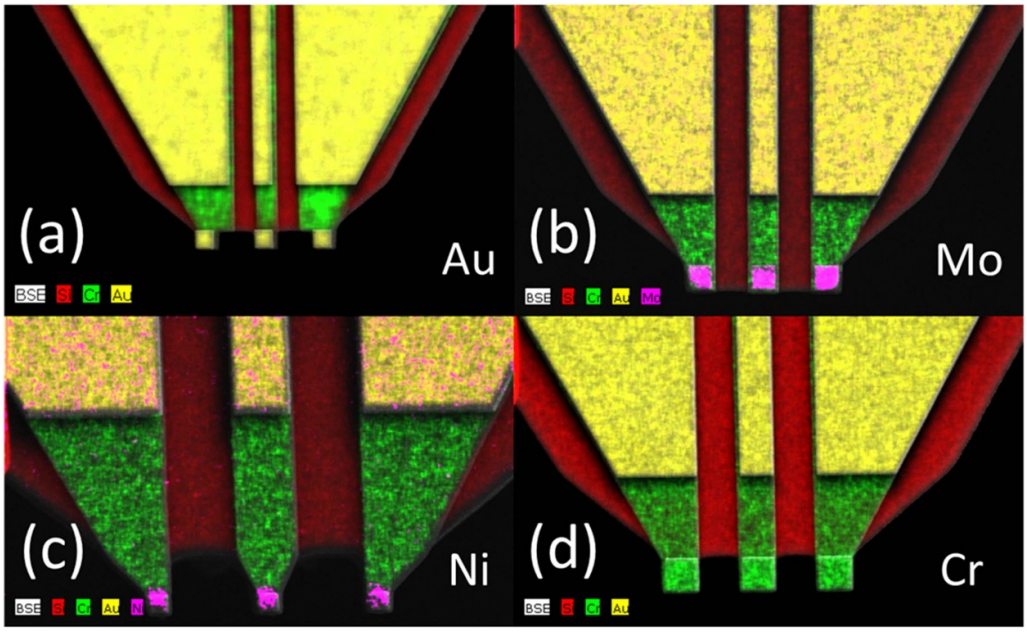

Figure 3. Images obtained during SEM from backscattered electrons showing the materials which make up the probes. The small contact metals are evaporated (a) gold, (b) molybdenum, (c) nickel, and (d) chromium.

Table 2. Measured arithmetic average surface roughness *Ra* of the evaporated pad metals—values obtained using analysis of AFM. The evaporation rate of the metallization is also given.

Pad metal	Evaporation rate (nm s^{-1})	*Ra* (nm)
Gold (Au)	1	3.61
Molybdenum (Mo)	0.2	1.03
Nickel (Ni)	0.4	1.11
Chromium (Cr)	0.2	2.79

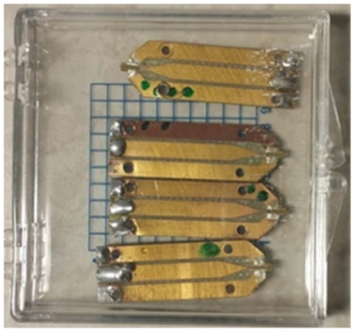

Figure 4. The microfabricated GSG probes mounted onto PCB for DC characterization.

were patterned onto the wafer at the same time as the GSG probes—this enabled an accurate determination of the series resistance associated with the ground and signal lines of the wafer probes. An accurate determination of the series resistance associated with each metallization enables the contact resistance of the individual pads to be estimated.

3.3. Electrical characterization of single microfabricated probes

The probes were measured in an in-house microwave characterization setup involving SEM and nanometric positioning which has been described in detail by the authors [34]. Importantly, this set up allowed us to carefully control the probe position in the z direction in steps as low as 10 nm—enabling the deflection of the probe's silicon microcantilever to be recorded. We are also able to control the tilt angle of the probes so that the three contact pads can be simultaneously in contact with the underlying surface. Knowledge of the microcantilever deflection and its geometry enables the force at the probe tip to be estimated. Briefly, the probe tip was moved approximately into its target area on the chip (an evaporated 500 nm-thick gold layer on a commercial, polished silicon wafer surface) using the SEM live images. Following this, the tip was lowered in nanometric steps until an initial electrical resistance value was recorded on a multimeter (Keithley, USA)—this value of z was considered to be zero deflection of the microcantilever. The probe was then subsequently lower in small (nanometric) steps and the electrical resistance was recorded between the grounds and the signal and the grounds.

Figure 6 shows an example of a probe in use—figure 6(a)—and an SEM images of a probe (Ni—0.6 μm) following testing—figure 6(b). The traces in the gold coating on the silicon chip surface are the touchdown of the probes—see red circles on figure 6(a). The mechanical contacting of the probes three contacts with the gold surface result in classic skate touchdown tracks also observed with commercial macroscopic probes. The marks are larger than the contact probes surface as the SEM images are taken after maximum force was exerted

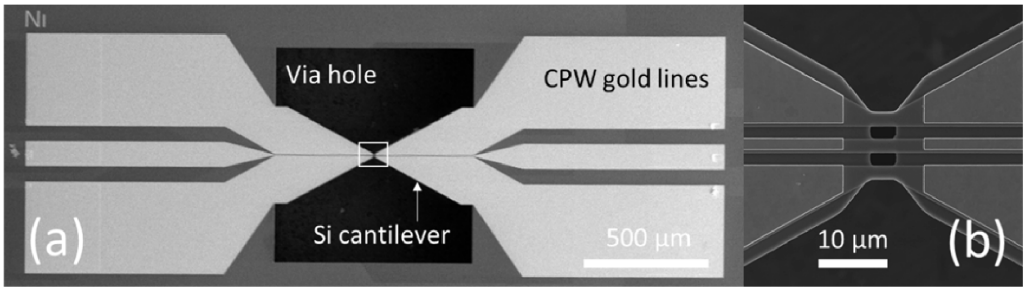

Figure 5. SEM images of (a) a back-to-back probe structure and (b) zoom on the central suspended section—white rectangle in (a). The inset to (b) is an example of cracking which was observed in some narrow, suspended structures.

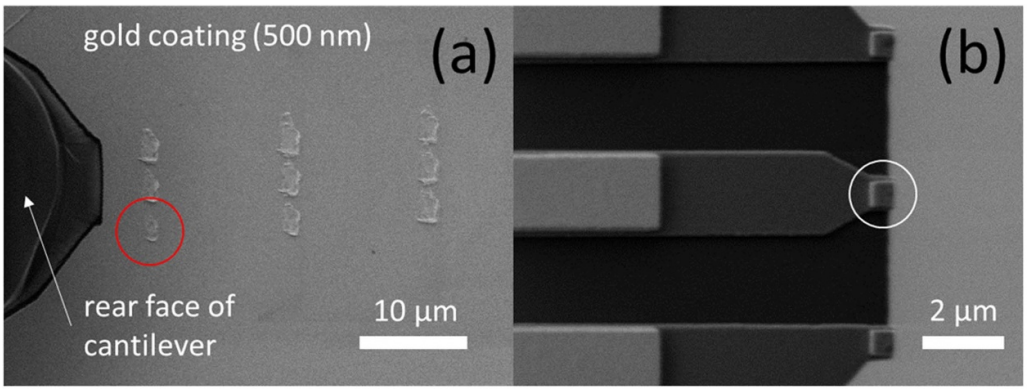

Figure 6. SEM images of (a) a microfabricated GSG probe contacting a gold-coated (500 nm) silicon wafer, and (b) a probe after use (Ni—0.6 μm). The red circle indicates the touchdown skate (<1 μm) resulting from contacting—in this case for an overtravel of $\sim$1 μm. The probe's contact pads are indicated by the red circle.

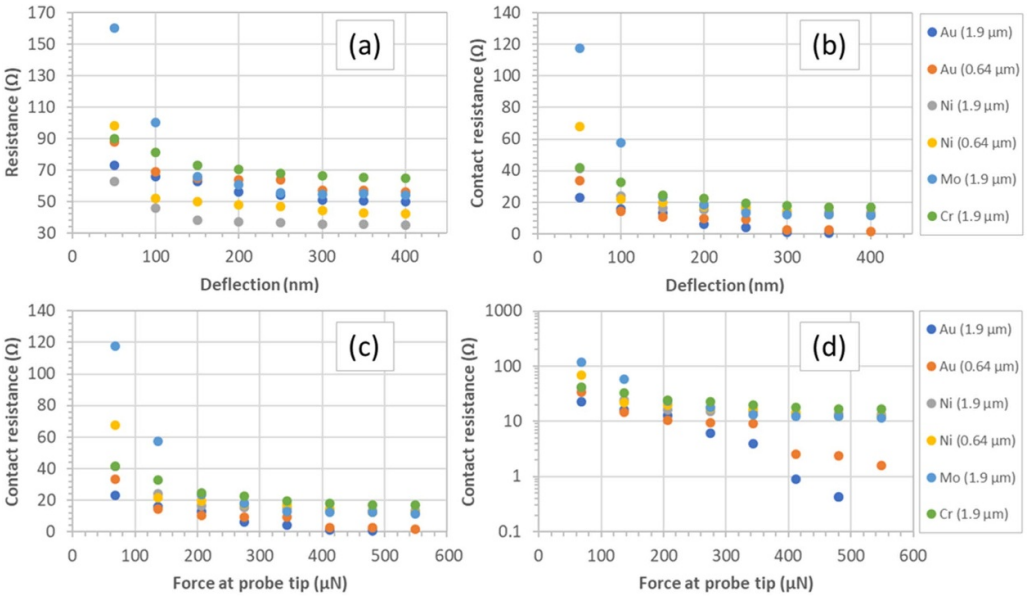

Figure 7. Variation of (a) and (b) the measured probe resistance with cantilever deflection and (c) and (d) the contact resistance with force (load) at the probe tip. The contact pad metallization is indicated by a colour given in the figure legend. The square contact pad size is also indicated in the figure legend.

at the probe tip—this is common in microwave probing. When the probes are used with a lower tip force, the probes do not indicate any visible signs of damage after 20 touchdowns—see white circle in figure 6(b).

Figure 7 shows the measured probe resistance and contact resistance as a function of probe deflection and tip force. For all metal types and probe contact pad sizes the resistance falls with increasing probe deflection—see figure 7(a).

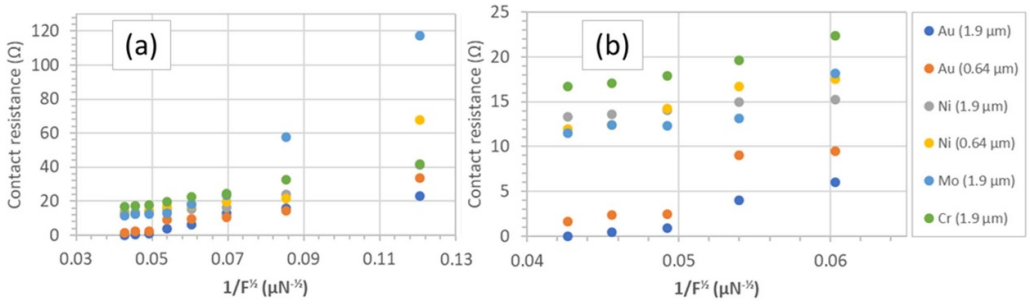

Figure 8. The contact resistance plotted as a function of $1/\sqrt{F}$ over the whole tip force range (a) and at the higher forces (b).

There appears to be two distinct variations of how the resistance varies with deflection for deflections greater or less than 200 nm. This is more apparent if the probe resistance is plotted logarithmically—see figure 7(b). By using the values of line resistance obtained from the back-to-back probes, the contact resistance can be evaluated from the probe resistance. In addition to this, the force at the probe tip can be evaluated as a function of probe deflection by assuming that the probe is a triangular cantilever [60]. The stiffness κ of a triangular cantilever can be approximated using the following formula:

$$\kappa = \frac{Et^3 w_b}{6l^3} \tag{1}$$

where E is the Young's modulus of the cantilever material, t is the cantilevr thickness, w_b is the width of the base anchoring of the triangular cantilever, and l is the perpendicular length of the triangular cantilever. The contact force at the tip F is given by:

$$F = \delta\kappa \tag{2}$$

where δ is the cantilever tip displacement. This enables the contact resistance of the contact pads to be plotted as a function of tip force—see figure 7(c). Again, two distinct variations of the contact resistance are visible when plotted logarithmically—see figure 7(d). A tip deflection of 200 nm equates to a tip force of ∼275 μN.

Figure 8 shows the contact resistance of the probe pads plotted as a function of the inverse of the square root of the frequency. The reason for this plotting will become apparent later when the contact resistivity is modelled.

Figure 9 shows a plot of what we define as the 'contact line resistivity' (defined as R_cL) as a function of cantilever deflection and tip force. It was found that a calculation of the contact resistivity (R_cA)—where A is the pad area—was not coherent with the results for different sized pads of the same material. However, if we consider that just the edge of the pad (length L) is in contact with the surface, then the results for different pad sizes of the same metal are coherent. This interpretation also has a practical significance. For ridged cantilever-based probes having small metal pads at their tips, the results here indicate that it is the length of the contact pad which plays a role in the total contact resistance rather than the area of the small pad.

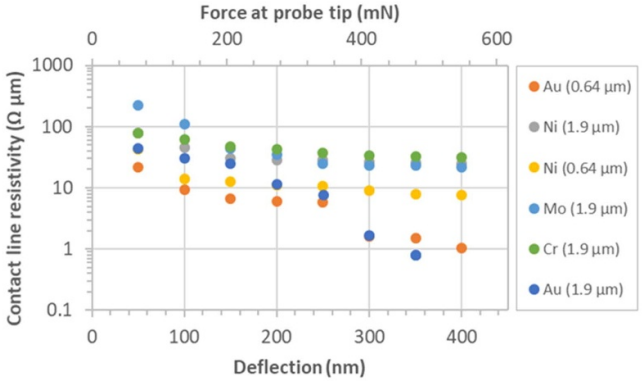

Figure 9. The contact line resistivity (Ω μm) plotted as a function of tip deflection and force. The contact line resistivity is defined as R_cL—where L is the length of the contact pad which is in contact with the surface.

The idea is best described by an illustration—see figure 10. Figure 10(a) shows the case of a thin relatively flexible cantilever (thickness t typically 1 μm) and figure 10(b) shows the case of a thick rigid cantilever (t typically 20 μm). There are advantages and disadvantages to using both for probes having well-defined metal pads at the end. In the case of a thin cantilever, bending is easily achieved—this means that the surface of the metal pad can be quasi-parallel to the wafer surface implying a large contact area. However, a thin cantilever may mean that the contact force is not enough to achieve a low contact resistance. In addition to this, bending of the thin cantilever—to achieve a higher force—may result in damage to microwave pads integrated on the cantilever. In contrast, the use of a thick, more rigid cantilever mean that sufficient contact force is reached for var little bending. However, the lack of bending means that only a portion of the contact pad surface will be in contact with the wafer surface. Figure 10(b) schematically illustrates the idea of the pad edge (of length L) in contact with the surface for a rigid cantilever. Evidently, little bending in this case means that any circuitry on the cantilever will be exposed to little mechanical strain—thus minimising the risk of damage.

The contact resistance R_c of a metal-to-metal contact under plastic deformation can be approximated by the following relationship [54, 55]:

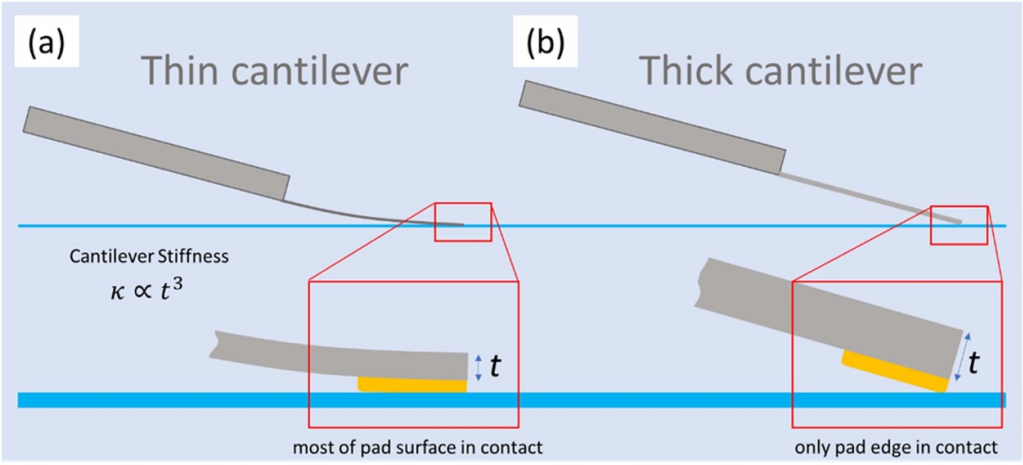

Figure 10. Comparison of using (a) a thin (relatively flexible) cantilever and (b) a thick (rigid) cantilever for a probe contacting an electrical contact pad.

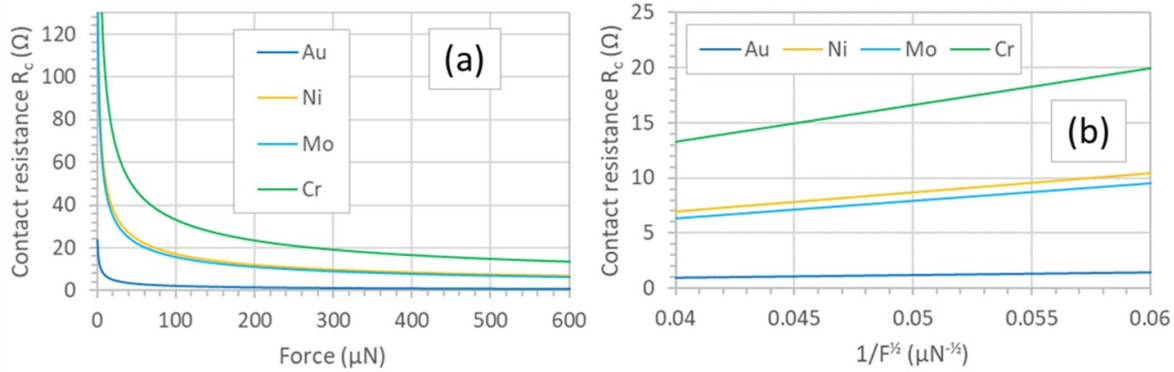

Figure 11. Modelling of the contact resistance. (a) Contact resistance as a function of force (load) and (b) contact resistance plotted as a function of $1/\sqrt{F}$. The thin film resistivity and micro-hardness of the four thin film mentalizations are used for the model.

$$R_c = \sqrt{\frac{\pi \rho^2 \eta H}{4F}} \tag{3}$$

where ρ is the resistivity of the metal, η is an empirical fitting constant, H is the hardness, and F is the force. The validity of this approximation has been demonstrated for many metal-to-metal types and contact size scales. Figure 11 shows equation (3) plotted graphically for the four different contact ad metals used here. The electrical resistivity and hardness of the thin films shown in table 1 are used. The value of the empirical fitting constant η is 1000. If we compare figure 7(c) with figure 10(a) and figure 8(b) with figure 10(b), it is apparent that the analytical model predicts the trends seen in the experimental results.

4. Discussions

4.1. Comparison with metal-to-metal electrical contacts

The electrical properties of metal-to-metal contacts under loading has been studied for many years now [61]. Concerning small metal-to-metal contacts, there have been many studies over the years in the context of MEMS [62–67] and RF MEMS [68–70]. It has been shown that contact forces in MEMS metal-metal contacts are typically in the range μN to mN [63] to achieve a minimum, stable electrical contact resistance. Previous work has demonstrated that gold-gold contacts require at least 60 μN for contact resistances below 100 mΩ [71]. Patton and Zabinski [63] showed that a force of $\sim$200 μN is required to minimize the contact resistance of gold-to-gold contacts (1.6 mm diameter steel balls coated with 1 μm thick sputtered gold—roughness 13.6 nm) onto GaAs coated with sputtered gold surface roughness 17.6 nm. Hyman and Mehregany [71] used gold-plated tungsten points having a contact area ranging from 0.5–7 μm^2 brought into contact with flat gold surfaces. They observed that a force of >100 μN was required to achieve a minimum and stable contact resistance. Jensen *et al* [72] used $\sim$50 μN to achieve a stable contact. Interestingly, they found that cycling at room temperature led to increase of contact resistance.

It is not evident to directly compared electrical behaviour of metal-to-metal contacts under load for several reasons including sample size, sample preparation, surface roughness and specific surface condition (cleanliness, oxidation…).

However, we can try to compare our results to those of others by calculating the practical contact resistivity based on specific sample size (the macroscopic sample area). In addition, technologically speaking, this has practical value as it can be used to estimate the contact resistance expected for a given contact pad size. Cuthrell and Tipping [73] measured resistance of 0.4 mΩ at a force of 784 mN for gold-to-gold contacts under loading—using their quoted sample contact area, a contact resistivity of 5.1 Ω μm^2 can be estimated. Pashley *et al* [74] measured resistances of 0.9 Ω when loading with 28 μN force range—W-Ni contacts gave considerable higher contact resistances explained by the presence of oxide surface layers. Hyman and Mehregany [71] measured electrical resistance varying from 250 to 80 mΩ for loads varying from 50 to 400 μN. based on their sample area, the contact resistivity can be estimated to be 0.2–0.06 Ω μm^2. Laurvick and Coutu [75] measured a contact resistance of 0.15 Ω when applying a load of 40 μN. Again, by using their sample size, this equates to a contact resistivity of 7.5 Ω μm^2. Yunus *et al* [76, 77] studied the electrical contact of gold-coated carbon nanotubes at low forces <1 mN and compared them with gold-gold contacts. They found contact resistance of the order of 0.4 Ω requires a force of >0.1 mN for gold-gold contacts. Kwon *et al* [78] compared gold-to-gold contacts with others. The resistance of a gold-to-gold contact was ∼0.15 Ω at a load of 1 mN—an order of magnitude lower than Pt-Pt contacts, ad lower than Iridium-Iridium and Gold-Iridium. Kwon *et al* [78] showed that gold-to-gold microcontacts have the lowest contact resistance (at 50 mN) but failed at an order of magnitude lower of contact cycles that Au-to-Pt and Au-to-Ir, and two orders of magnitude lower than Au–Pt alloy and Ir-to-Ir. However, the Au-to-Au contacts endured for 10^5 contact cycles—in the context of commercial microwave probe touchdown this is large. We have previous demonstrated touchdown cycling of MEMS-based GSG probes [37]. We have previously measured the resistance of gold/silicon cantilever-based probes at higher tip forces [38]. A contact resistance as low as 0.14 Ω was recorded at a tip deflection of 800 nm (corresponding to a tip force of ∼1.1 mN). For a tip deflection of 50 nm (contact force = 70 μN) [33], the measured electrical resistance was 4 Ω—comparable with to the data for gold probes in the present study.

4.2. Comparison with probe card technologies for low frequency measurements

We can also compare our findings with probe card technologies. Kim *et al* [79] fabricated and tested Ni based probes having a 70–100 μm pitch; using a contact force of 118 mN they measured a contact resistance of <1 Ω. Kandalaft *et al* [80] used a MEMS-based approach to produce wafer probes having a contact resistance of 11.3 mΩ using a small force—the contact pad size was 40 × 70 μm. they also noted less damage to on-wafer contact pads compared to the work of others due to low-force, optimised contacting. Kim and Kim [81] fabricated probes with Ni/Co alloy contacts with a contact area of 10 × 10 μm contacts, minimum contact resistance was achieved at a contact force of 15 mN (147 MPa). Kataoka *et al* [82] fabricated and tested Ni based probes having a contact are of 40 × 212 μm using contact forces between 10 and 1000 μN; they measured a contact resistance of 0.64 Ω when contacting to on aluminium pads at a contact force of 10 μN. Kataoka *et al* [83] fabricated and measured Ni based tips with a pitch of 250 μm pitch; using a contact force of 10 mN when probing aluminium pads they measured a contact resistance <3 Ω for 10 000 contact cycles. Using Ni and Ni–Co based probe contacts, Kim *et al* [84] mesred a contact resistance of 0.2 Ω for a contact force of 14 mN using 50 μm probe pitch for 10 000 touchdowns. Kim *et al* [85] mechanically tested the robustness of Ni-B based probes having a contact area of 80 × 50 μm contacts and contact forces 5–100 mN.

4.3. Comparison with RF probing technologies

In terms of commercially-available RF probes, GGB Picoprobe supply Be/Cu/W tips which have a 50 μm pitch and 1 dB insertion loss (IL) at a maximum frequency of 50 GHz [86]. T-plus probes supply Ni alloy tips with an IL of 0.5 dB at 25 GHz [87]. MPI Multi-contact probes supply Ti coated tips with an IL of 1 dB at 6 GHz [88]. Yokowo Connectors supply Au/Pd alloy tips with a 130 μm pitch with an IL of 1 dB at 6 GHz [89]. Pasternack probes supply Au tips with a 800 μm pith and an IL of 0.5 dB at 40 GHz [90]. Finally, Marinissen *et al* [91] demonstrated Ni alloy (Cascade Microtech. Formfactor) probes with a contact resistance of 2.1 Ω and a pitch of 50 μm [92]. Recently Lee *et al* [93] fabricated and tested a non-MEMS spring-based pin Be/Cu probes approach having a pitch of 350 μm; this demonstrates that despite large contact areas and pitches, the non-MEMS based approach is still in use.

In the context of surface contact probes having metal-to-metal electrical contacts we can define two displacement parameters: the 'overtravel' and the 'skate'. The overtravel refers to the vertical displacement of the probe to achieve a minimum contact resistance whereas the skate corresponds to the lateral distance the probe pads travel along the wafer contact pad once the probe is in contact with the pad. An example is the Cascade infinity XT probe (Formfactor, USA) [92] which has a typical overtravel of 50 μm resulting in a skate of 20 μm at 10 gf (a contact force of ∼98 mN providing a contact resistance equal to 0.05 Ω). We can compare these figures to our results. Using our micromachined probe, an overtravel of 400 nm results in a skate of <1 μm at a contact force of 550 μN (contact resistance <1 Ω—the contact force being considerably smaller than commercial probes).

5. Conclusions

Using a MEMS approach for the fabrication of miniaturized GSG wafer probes, it is possible to estimate the contact resistance of well-defined sub-micrometre-sized metal 'mesa' contact pads destined for metal-to-metal on-wafer circuit contacting. The lithographic approach enables the evaporated pad metal type to be easily varied and its size. The wafer probe contact pad size is 3.6 and 0.36 μm^2. The

micro/nanofabrication approach also enables many probes to be manufactured—enabling the reproducibility of the results to be evaluated. Using rigid MEMS cantilevers (>1000 Nm^{-1}), the contact resistance of small metal pads is associated with the lateral pad length which is in contact with the surface rather than the pad area. Our findings suggest that in such probes a contact line resistivity can be defined which is associated with the pad contact edge which is in contact with the underlying metal surface, e.g. an on-wafer pad. Gold pads having a contact length of <2 μm have a contact resistance of <1 and <2 Ω for a sub-micrometre pad length at a tip force of ~400 μN. The other metals (Ni, Mo, and Cr) had a higher contact resistance ~10 Ω at a tip force of 400 μN—but may be of use if harder contacts are required e.g. on aluminium. On a practical note, for a rigid cantilever it is found that a cantilever deflection (i.e. the probe overtravel) of ~300 nm is enough to achieve a stable low contact resistance—meaning damage to pads (probe and on-wafer) can be minimised due to resulting the low skate. The maximum touchdown skate length for the wafer probes is of the order of 1 μm—somewhat smaller than commercial probes. A sub-micrometre-sized gold pad on a rigid cantilever appears to be a suitable candidate contact for miniaturized microwave probes fabricated using MEMS technologies.

Data availability statement

The data that support the findings of this study are available upon reasonable request from the authors.

Acknowledgments

The authors would like to thank the following people for technical help: François Vaurette, Annie Fattorini, and Dmitri Yarekha. We would also like to thank Flavie Braud for the manufacture of certain objects used in the mounting of the chips. We thank Sophie Barois for help with the microwave measurements and Dominique Desremes for help with the AFM. This work was financially supported by a French 'Equipex' project 'Excelsior' and partially supported by the French RENATECH network.

ORCID iD

Steve Arscott https://orcid.org/0000-0001-9938-2683

References

[1] Rumiantsev A and Doerner R 2013 RF probe technology: history and selected topics *IEEE Microw. Mag.* **14** 46–58
[2] El Fellahi A, Haddadi K, Marzouk J, Arscott S, Boyaval C, Lasri T and Dambrine G 2015 Integrated MEMS RF probe for SEM station—pad size and parasitic capacitance reduction *IEEE Microw. Wirel. Compon. Lett.* **25** 693–5
[3] Xiao M *et al* 2017 Millimeter wave communications for future mobile networks *IEEE J. Sel. Areas Commun.* **35** 1909–35
[4] Rappaport T S, Xing Y, Kanhere O, Ju S, Madanayake A, Mandal S, Alkhateeb A and Trichopoulos G C 2019 Wireless communications and applications above 100 GHz: opportunities and challenges for 6G and beyond *IEEE Access* **7** 78729–57
[5] Remley K A *et al* 2017 Measurement challenges for 5G and beyond: an update from the national institute of standards and technology *IEEE Microw. Mag.* **18** 41–56
[6] Horibe M, Kato Y and Sakamaki R 2020 Electromagnetic measurement techniques for materials and device used in 6G wireless communications *2020 2nd 6G Wireless Summit (6G SUMMIT)* (Levi: IEEE) pp 1–5
[7] Wartenberg S A 2003 Selected topics in RF coplanar probing *IEEE Trans. Microw. Theory Tech.* **51** 1413–21
[8] Leslie B and Matta F 1988 Membrane probe card technology *Proc. IEEE Int. Test Conf.* pp 601–7
[9] Hong S, Lee K and Bravman J C 1989 Design and fabrication of a monolithic high-density probe card for high-frequency on-wafer testing *Int. Technical Digest on Electron Devices Meeting* (Washington, DC: IEEE) pp 289–92
[10] Hong S, Weihs T P, Kwon O K and Bravman J C 1989 Cantilever beam micro-contacts in a multi-chip interconnection system *Proc. Seventh IEEE/CHMT Int. Electronic Manufacturing Technology Symp.* (San Francisco, CA: IEEE) pp 239–45
[11] Godshalk E M 1993 A W-band wafer probe *1993 IEEE MTT-S Int. Microwave Symp. Digest* (Atlanta, GA: IEEE) pp 171–4
[12] Beiley M, Leung J and Wong S S 1995 A micromachined array probe card-fabrication process *IEEE Trans. Compon. Packag. Manuf. Technol.* B **18** 179–83
[13] Beiley M, Leung J and Wong S S 1995 A micromachined array probe card-characterization *IEEE Trans. Compon. Packag. Manuf. Technol.* B **18** 184–91
[14] SafWat A M E, Andrews M, Hayden L, Gleason K R and Strid E 2002 A probe technology for 110+ GHz integrated circuits with aluminum pads *59th ARFTG Conf. Digest, Spring 2002* (Seattle, WA: IEEE) pp 60–66
[15] Chun D, Ang S S, Hanhua F, Tay A A O, Rotaru M D, Keezer D and Tan J P H 2003 A MEMS based interposer for nano-wafer level packaging test *Proc. 5th Electronics Packaging Technology Conf. (EPTC 2003)* (Singapore: IEEE) pp 405–9
[16] Itoh T, Kawamura S, Kataoka K and Suga T 2003 Contact properties of micromachined Ni probes *Proc. Forty-Ninth IEEE Holm Conf. on Electrical Contacts, 2003* (Washington, DC: IEEE) pp 223–7
[17] Itoh T, Kawamura S, Kataoka K and Suga T 2005 Electroplated Ni microcantilever probe with electrostatic actuation *Sens. Actuators* **123–124** 490–6
[18] Kim Y-M K, Yoon H-C Y and Lee J-H L 2005 Silicon micro-probe card using porous silicon micromachining technology *ETRI J.* **27** 433–8
[19] Tsou C, Huang S-L, Li H and Lai T 2006 Electroplated nickel micromachined probes with out-of-plane predeformation for IC chip testing *J. Micromech. Microeng.* **16** 2197–202
[20] Liu J, Noman M, Bain J A, Schlesinger T E and Fedder G K 2008 CMOS-MEMS probes for reconfigurable ICs *2008 IEEE 21st Int. Conf. on Micro Electro Mechanical Systems* (Tucson, AZ: IEEE) pp 515–8
[21] Wang F, Cheng R and Li X 2009 MEMS vertical probe cards with ultra densely arrayed metal probes for wafer-level IC testing *J. Microelectromech. Syst.* **18** 933–41
[22] Reck T J, Chen L, Zhang C, Groppi C, Xu H, Arsenovic A, Barker N S, Lichtenberger A and Weikle R M 2010 Micromachined on-wafer probes *2010 IEEE/MTT-S Int. Microwave Symp.—MTT 2010* (Anaheim, CA: IEEE) pp 65–68

[23] Reck T J, Chen L, Zhang C, Arsenovic A, Groppi C, Lichtenberger A W, Weikle R M and Barker N S 2011 Micromachined probes for submillimeter-wave on-wafer measurements—part I: mechanical design and characterization *IEEE Trans. Terahertz Sci. Technol.* **1** 349–56
[24] Reck T J, Chen L, Zhang C, Arsenovic A, Groppi C, Lichtenberger A, Weikle R M and Barker N S 2011 Micromachined probes for submillimeter-wave on-wafer measurements—part II: RF design and characterization *IEEE Trans. Terahertz Sci. Technol.* **1** 357–63
[25] Chen L, Zhang C, Reck T J, Groppil C, Arsenovic A, Lichtenberger A, Weikle R M and Barker N S 2011 Terahertz micromachined on-wafer probes: repeatability and robustness *2011 IEEE/MTT-S Int. Microwave Symp.—MTT 2011* (Baltimore, MD: IEEE) pp 1–4
[26] Yu Q, Bauwens M F, Zhang C, Lichtenberger A W, Weikle R M and Barker N S 2013 Improved micromachined terahertz on-wafer probe using integrated strain sensor *IEEE Trans. Microw. Theory Tech.* **61** 4613–20
[27] Yu Q, Bauwens M, Zhang C, Lichtenberger A W, Weikle R M and Barker N S 2013 Integrated strain sensor for micromachined terahertz on-wafer probe *2013 IEEE/MTT-S Int. Microwave Symp.—MTT 2013* (Seattle, WA: IEEE) pp 1–4
[28] Yuan T, Chen D, Chen J, Fu H, Kurth S, Otto T and Gessner T 2013 Design, fabrication and characterization of MEMS probe card for fine pitch IC testing *Sens. Actuators* **204** 67–73
[29] Bauwens M F, Alijabbari N, Lichtenberger A W, Barker N S and Weikle R M 2014 A 1.1 THz micromachined on-wafer probe *2014 IEEE/MTT-S Int. Microwave Symp.—MTT 2014* (Tampa, FL: IEEE) pp 1–4
[30] Bauwens M F, Chen L, Zhang C, Arsenovic A I, Alijabbari N, Lichtenberger A W, Barker N S and Weikle I I R M 2014 Characterization of micromachined on-wafer probes for the 600–900 GHz waveguide band *IEEE Trans. Terahertz Sci. Technol.* **4** 527–9
[31] Marzouk J, Arscott S, Haddadi K, Lasri T and Dambrine G 2014 Miniaturized MEMS-based GSG probes for microwave characterization *2014 44th European Microwave Conf. (EuMC)* (Rome: IEEE) pp 1150–3
[32] Marzouk J, Arscott S, Haddadi K, Lasri T, Boyaval C, Lepilliet S and Dambrine G 2014 Miniaturized microcantilever-based RF microwave probes using MEMS technologies *Proc. Eng.* **87** 692–5
[33] Marzouk J, Arscott S, Fellahi A E, Haddadi K, Lasri T, Boyaval C and Dambrine G 2015 MEMS probes for on-wafer RF microwave characterization of future microelectronics: design, fabrication and characterization *J. Micromech. Microeng.* **25** 075024
[34] Haddadi K, El Fellahi A, Marzouk J, Arscott S, Boyaval C, Lasri T and Dambrine G 2015 Robotic on-wafer probe station for microwave characterization in a scanning electron microscope *2015 IEEE MTT-S Int. Microwave Symp. (IMS2015)* (Phoenix, AZ: IEEE) pp 1–3
[35] El Fellahi A, Haddadi K, Marzouk J, Arscott S, Boyaval C, Lasri T and Dambrine G 2015 Nanorobotic RF probe station for calibrated on-wafer measurements *2015 European Microwave Conf. (EuMC 2015)* (Paris: IEEE) pp 163–6
[36] El Fellahi A, Haddadi K, Marzouk J, Arscott S, Boyaval C, Lasri T and Dambrine G 2015 On-wafer probe station for microwave metrology at the nanoscale *2015 IEEE Int. Instrumentation and Measurement Technology Conf. (I2MTC) Proc.* (Pisa: IEEE) pp 1960–4
[37] Marzouk J, Arscott S, El Fellahi A, Haddadi K, Lasri T, Buchaillot L and Dambrine G 2015 MEMS-based RF probes for on-wafer microwave characterization of micro/nanoelectronics *28th IEEE Int. Conf. on Micro Electro Mechanical Systems (MEMS)* (Estoril: IEEE) pp 1012–5
[38] Marzouk J, Arscott S, El Fellahi A, Haddadi K, Boyaval C, Lepilliet S, Lasri T and Dambrine G 2016 Optimization of a microelectromechanical systems (MEMS) approach for miniaturized microcantilever-based RF microwave probes *Sens. Actuators* **238** 51–59
[39] Daffe K, Marzouk J, Fellahi A E, Xu T, Boyaval C, Eliet S, Grandidier B, Arscott S, Dambrine G and Haddadi K 2017 Nano-probing station incorporating MEMS probes for 1D device RF on-wafer characterization *2017 47th European Microwave Conf. (EuMC)* (Nuremberg: IEEE) pp 831–4
[40] Marzouk J, Avramovic V and Arscott S 2020 Intertrack surface losses in miniature coplanar waveguide on silicon-on-insulator *J. Phys. D: Appl. Phys.* **54** 045102
[41] Taleb A, Pomorski D, Boyaval C, Arscott S, Dambrine G and Haddadi K 2020 Control and automation for miniaturized microwave GSG nanoprobing *Machine Vision and Navigation* ed O Sergiyenko, W Flores-Fuentes and P Mercorelli (Cham: Springer International Publishing) pp 751–68
[42] Zhang C, Bauwens M, Barker N S, Weikle R M and Lichtenberger A W 2016 A W-band micromachined on-wafer probe with integrated balun for characterization of differential circuits *IEEE Trans. Microw. Theory Tech.* **64** 1585–93
[43] Scott Barker N, Bauwens M, Lichtenberger A and Weikle R 2017 Silicon-on-insulator substrates as a micromachining platform for advanced terahertz circuits *Proc. IEEE* **105** 1105–20
[44] Gonzalez B D, Bauwens M F, Zhang C, Lichtenberger A W, Barker N S and Weikle R M 2016 A 0–40 GHz on-wafer probe with replaceable micromachined silicon tip *IEEE Microw. Wirel. Compon. Lett.* **26** 110–2
[45] Zhang C, Bauwens M F, Xie L, Cyberey M E, Barker N S, Weikle R M and Lichtenberger A W 2017 A micromachined differential probe for on-wafer measurements in the WM-1295 (140–220 GHz) band *2017 IEEE/MTT-S Int. Microwave Symp.—IMS 2017* (Honolulu, HI: IEEE) pp 1088–90
[46] Zhang C, Bauwens M, Cyberey M E, Xie L, Lichtenberger A W, Scott Barker N and Weikle R M 2019 A differential probe with integrated balun for on-wafer measurements in the WR-3.4 (220–330 GHz) waveguide band *2019 IEEE/MTT-S Int. Microwave Symp.—IMS 2019* (Boston, MA: IEEE) pp 1269–71
[47] Phung G N, Schmuckle F J, Doerner R, Kahne B, Fritzsch T, Arz U and Heinrich W 2019 Influence of microwave probes on calibrated on-wafer measurements *IEEE Trans. Microw. Theory Tech.* **67** 1892–900
[48] Phung G N and Arz U 2020 Parasitic probe effects in measurements of coplanar waveguides with narrow ground width *2020 IEEE 24th Workshop on Signal and Power Integrity (SPI)* (Cologne: IEEE) pp 1–4
[49] Bustillo J M, Howe R T and Muller R S 1998 Surface micromachining for microelectromechanical systems *Proc. IEEE* **86** 1552–74
[50] Kovacs G T A, Maluf N I and Petersen K E 1998 Bulk micromachining of silicon *Proc. IEEE* **86** 1536–51
[51] Judy J W 2001 Microelectromechanical systems (MEMS): fabrication, design and applications *Smart Mater. Struct.* **10** 1115–34
[52] Albrecht T R, Akamine S, Carver T E and Quate C F 1990 Microfabrication of cantilever styli for the atomic force microscope *J. Vac. Sci. Technol. Vac. Surf. Films* **8** 3386–96
[53] Walker M J 2001 Comparison of Bosch and cryogenic processes for patterning high-aspect-ratio features in silicon *Microelectronic and MEMS Technologies* ed U F W

Behringer and D G Uttamchandani (Edinburgh: International Society for Optics and Photonics) pp 89–99
[54] Holm R and Holm E 1967 *Electric Contacts: Theory and Application* (Berlin: Springer)
[55] Slade P G 2014 *Electrical Contacts: Principles and Applications* (Boca Raton, FL: CRC Press)
[56] Pruitt B L, Park W-T and Kenny T W 2004 Measurement system for low force and small displacement contacts *J. Microelectromech. Syst.* **13** 220–9
[57] Yoder K B, Elmustafa A A, Lin J C, Hoffman R A and Stone D S 2003 Activation analysis of deformation in evaporated molybdenum thin films *J. Phys. D: Appl. Phys.* **36** 884–95
[58] Pauleau Y, Kukielka S, Gulbinski W, Ortega L and Dub S N 2006 Structure and physical properties of nickel films deposited by microwave plasma-assisted cathodic sputtering *J. Phys. D: Appl. Phys.* **39** 2803–8
[59] Kataria S, Goyal S, Dash S and Tyagi A K 2010 Nanomechanical characterization of thermally evaporated Cr thin films—FE analysis of the substrate effect *Thin Solid Films* **519** 312–8
[60] Sader J E and White L 1993 Theoretical analysis of the static deflection of plates for atomic force microscope applications *J. Appl. Phys.* **74** 1–9
[61] Bowden F P and Tabor D 1939 The area of contact between stationary and moving surfaces *Proc. R. Soc.* A **169** 391–413
[62] Coutu R A, Kladitis P E, Leedy K D and Crane R L 2004 Selecting metal alloy electric contact materials for MEMS switches *J. Micromech. Microeng.* **14** 1157–64
[63] Patton S T and Zabinski J S 2005 Fundamental studies of Au contacts in MEMS RF switches *Tribol. Lett.* **18** 215–30
[64] Kim S H, Asay D B and Dugger M T 2007 Nanotribology and MEMS *Nano Today* **2** 22–29
[65] Yang Z, Lichtenwalner D J, Morris A S, Krim J and Kingon A I 2009 Comparison of Au and Au–Ni alloys as contact materials for MEMS switches *J. Microelectromech. Syst.* **18** 287–95
[66] Toler B F, Coutu R A and McBride J W 2013 A review of micro-contact physics for microelectromechanical systems (MEMS) metal contact switches *J. Micromech. Microeng.* **23** 103001
[67] Basu A, Adams G G and McGruer N E 2016 A review of micro-contact physics, materials, and failure mechanisms in direct-contact RF MEMS switches *J. Micromech. Microeng.* **26** 104004
[68] Rezvanian O, Zikry M A, Brown C and Krim J 2007 Surface roughness, asperity contact and gold RF MEMS switch behavior *J. Micromech. Microeng.* **17** 2006–15
[69] Iannacci J 2018 RF-MEMS technology as an enabler of 5G: low-loss ohmic switch tested up to 110 GHz *Sens. Actuators* **279** 624–9
[70] Liu Y, Liu J, Yu B and Liu X 2018 A compact single-cantilever multicontact RF-MEMS switch with enhanced reliability *IEEE Microw. Wirel. Compon. Lett.* **28** 191–3
[71] Hyman D and Mehregany M 1998 Contact physics of gold microcontacts for MEMS switches *Electrical Contacts—1998. Proc. Forty-Fourth IEEE Holm Conf. on Electrical Contacts (Cat. No.98CB36238)* (Arlington, VA: IEEE) pp 133–40
[72] Jensen B D, Chow L L-W, Huang K, Saitou K, Volakis J L and Kurabayashi K 2005 Effect of nanoscale heating on electrical transport in RF MEMS switch contacts *J. Microelectromech. Syst.* **14** 935–46
[73] Cuthrell R E and Tipping D W 1973 Electric contacts. II. Mechanics of closure for gold contacts *J. Appl. Phys.* **44** 4360–5
[74] Pashley M D, Pethica J B and Tabor D 1984 Adhesion and micromechanical properties of metal surfaces *Wear* **100** 7–31
[75] Laurvick T V and Coutu R A 2017 Improving gold/gold microcontact performance and reliability under low-frequency AC through circuit loading *IEEE Trans. Compon. Packag. Manuf. Technol.* **7** 345–53
[76] Yunus E M, McBride J W and Spearing S M 2007 The relationship between contact resistance and contact force on Au coated carbon nanotube surfaces *Electrical Contacts—2007 Proc. 53rd IEEE Holm Conf. on Electrical Contacts* (IEEE) pp 167–74
[77] Yunus E M, Spearing S M and McBride J W 2009 The relationship between contact resistance and contact force on Au-coated carbon nanotube surfaces under low force conditions *IEEE Trans. Compon. Packag. Technol.* **32** 650–7
[78] Kwon H, Choi D-J, Park J-H, Lee H-C, Park Y-H, Kim Y-D, Nam H-J, Joo Y-C and Bu J-U 2007 Contact materials and reliability for high power RF-MEMS switches *2007 IEEE 20th Int. Conf. on Micro Electro Mechanical Systems (MEMS)* (Hyogo: IEEE) pp 231–4
[79] Kim B-H, Park S, Lee B, Lee J-H, Min B-G, Choi S-D, Cho D-I and Chun K 2002 A novel MEMS silicon probe card *Technical Digest. MEMS 2002 IEEE Int. Conf. Fifteenth IEEE Int. Conf. on Micro Electro Mechanical Systems (Cat. No.02CH37266)* (Las Vegas, NV: IEEE) pp 368–71
[80] Kandalaft N, Basith I I and Rashidzadeh R 2014 Low-contact resistance probe card using MEMS technology *IEEE Trans. Instrum. Meas.* **63** 2882–9
[81] Kim B-H and Kim J-B 2008 Design and fabrication of a highly manufacturable MEMS probe card for high speed testing *J. Micromech. Microeng.* **18** 075031
[82] Kataoka K, Kawamura S, Itoh T, Suga T, Ishikawa K and Honma H 2002 Low contact-force and compliant MEMS probe card utilizing fritting contact *Technical Digest. MEMS 2002 IEEE Int. Conf. Fifteenth IEEE Int. Conf. on Micro Electro Mechanical Systems (Cat. No.02CH37266)* (Las Vegas, NV: IEEE) pp 364–7
[83] Kataoka K, Itoh T, Inoue K and Suga T 2004 Multi-layer electroplated micro-spring array for MEMS probe card *17th IEEE Int. Conf. on Micro Electro Mechanical Systems. Maastricht MEMS 2004 Technical Digest* (Maastricht: IEEE) pp 733–6
[84] Kim B-H, Kim H-C, Choi S-D, Chun K, Kim J-B and Kim J-H 2007 A robust MEMS probe card with vertical guide for a fine pitch test *J. Micromech. Microeng.* **17** 1350–9
[85] Kim K, Kwon H-B, Ahn H-R and Kim Y-J 2017 MEMS-based Ni–B probe with enhanced mechanical properties for fine pitch testing *Micro Nano Syst. Lett.* **5** 3
[86] (Available at: www.ggb.com) GGB Picoprobe
[87] (Available at: http://tplus-co.com/products01.html) T-plus probes
[88] (Available at: www.mpi-corporation.com/ast/mpi-rf-probes-accessories/titan-multicontact-probes) MPI Multi-contact probes
[89] (Available at: www.yokowo.co.jp/english/project/connector/circuit.html) Yokowo Connectors
[90] (Available at: www.pasternack.com/rf-coaxial-gsg-probe-800-micron-pitch-40ghzcable-mount-2.92mm-pe2pb1004-p.aspx) Pasternack
[91] Marinissen E J, Fodor F, De Wachter B, Kiesewetter J, Hill E and Smith K 2017 A fully automatic test system for characterizing large-array fine-pitch micro-bump probe cards *2017 Int. Test Conf. in Asia (ITC-Asia)* (Taipei: IEEE) pp 144–9
[92] (Available at: www.formfactor.com/products/probes) FormFactor
[93] Lee K M, Oh J H, Kim M S, Kim T S and Kim M 2021 RF pogo-pin probe card design aimed at automated millimeter-wave multi-port integrated-circuit testing *Electronics* **10** 2446